Network Coordinated Power Point Tracking for Grid-Connected Photovoltaic Systems

Xudong Wang, Yibo Pi, Wenguang Mao, and Hua Huang

***Abstract*—Maximum power point tracking (MPPT) achieves maximum power output for a photovoltaic (PV) system under various environmental conditions. It significantly improves the energy efficiency of a specific PV system. However, when an increasing number of PV systems are connected to a distribution grid, MPPT poses several risks to the grid: 1)** *over-voltage problem,* **i.e., voltage in the distribution grid exceeds its rating; 2)** *reverse power-flow problem,* **i.e., power that flows into the grid exceeds an allowed level. To solve these problems, power point tracking of all PV systems in the same distributed grid needs to be coordinated via a communication network. Thus, coordinated power point tracking (CPPT) is studied in this paper. Firstly, an optimization problem is formulated to determine the power points of all PV systems, subject to the constraints of voltage, reverse power flow, and fairness. Conditions that obtain the optimal solution are then derived. Secondly, based on these conditions, a distributed and practical CPPT scheme is developed. It coordinates power points of all PV systems via a communication network, such that: 1) voltage and reverse power flow are maintained at a normal level; 2) each PV system receives a fair share of surplus power. Thirdly, a wireless mesh network (WMN) is designed to support proper operation of the distributed CPPT scheme. CPPT is evaluated through simulations that consider close interactions between WMN and CPPT. Performance results show that: 1) CPPT significantly outperforms MPPT by gracefully avoiding both over-voltage and reverse power-flow problems; 2) CPPT achieves fair sharing of surplus power among all PV systems; 3) CPPT can be reliably conducted via a WMN.**

***Index Terms*—Coordinated power point tracking, photovoltaic system, smart grid communications, wireless mesh network**

I. Introduction

PHOTOVOLTAIC cells play a critical role in providing solar energy. Power plants based on PV cells have been built up in many countries. More interestingly, PV cells are being steadily adopted by residents and will be widely deployed in residential communities.

The output power of a PV cell can be affected by the operation environment such as solar irradiation and temperature. To improve energy efficiency, a maximum power point tracking (MPPT) algorithm [1] is usually implemented as a key function in the inverter to track the maximum power point on the I-V curve of a PV system[1]. A PV system with MPPT generates maximum solar energy under various operation environments. However, when such systems are connected to a distribution grid, stability issues arise.

Considering a distribution grid in Fig. 1, as the number of PV systems increases, the grid is exposed to a high risk of instability. More specially, when PV systems connected to the grid follow MPPT, there exist two problems. The first is the *over-voltage problem*, i.e., the voltage at a user can exceed its rating. Over-voltage usually happens when the output power of PV systems is more than the need of the local load and thus power flows into the grid. The second is the *reverse power-flow problem*. When the total output power of all PV systems in the grid exceeds the total loads in the grid, then power flows back to the grid through the transformer. Such a reverse power flow poses a few challenges. Firstly, the step-down transformer of the distribution grid needs to support reverse operation. Secondly, the reverse power flow is not stable and can be hardly dispatched, so a grid company either forbids reverse power flow or sets a limit to the amount of reverse power flow.

Since PV systems in the same distribution grid all make contributions to the above two problems, their power points need to be coordinated together by considering the behavior of the entire distribution grid. In order to deliver commands to or collect information from distributed PV systems, a communication network is required. Via this network, coordinated power point tracking (CPPT) is conducted. In general, CPPT includes two simple steps: 1) The power points of all PV systems are determined by a central controller, based on the overall status of the distribution grid; 2) The power points are sent to PV systems where each of them takes a local scheme to track the assigned power point. However, there exist several challenging issues in CPPT.

The *first issue* is how to determine the optimal power points for all PV systems. An optimization algorithm is needed to maximize output power of PV systems subject to the constraints of voltage and reverse power flow. However, it can lead to unfairness among PV systems. For example, when the over-voltage or reverse power-flow problem happens, different PV systems can be selected to reduce output power, but reducing output power of a particular user means less revenue for this user. To avoid unfair sharing of surplus power among different users, fairness must be taken into account in the optimization algorithm.

The *second issue* in CPPT is to design a practical and distributed algorithm that can follow the power points determined by the optimization algorithm. The distributed algorithm needs to converge quickly so that it is adaptive to varying loads in the distribution grid. Moreover, it must contain a mechanism

Xudong Wang, Yibo Pi, and Wenguang Mao are with the University of Michigan-Shanghai Jiao Tong University Joint Institute, Shanghai Jiao Tong University, Shanghai, China. Hua Huang is with Shanghai Electric Power Research Institute, State Grid Corporation of China. Corresponding author: Xudong Wang, Email: wxudong@ieee.org

[1]Throughout this paper, a PV system is a combination of the inverter and all PV cells that are installed by a user.

to immediately respond to over-voltage and maintain a normal voltage level.

The *third issue* in CPPT is to design a wireless network such that messages between the central control and PV systems can be reliably delivered to support proper operation of the distributed algorithm of CPPT. It is true that a wired network can deliver messages more reliably. However, for the sake of low cost and easy maintenance, actually a wireless network is preferred by CPPT.

All the above issues of CPPT have been resolved in this paper. First, an optimization problem is formulated to determine the optimal power point of each PV system, subject to three constraints: reverse power limit, voltage range, and fair sharing of surplus power. We then derive the condition under which the optimal solution is achieved. Based on this condition, a weighted max-min fair share algorithm [2] is developed to determine power points of PV systems in a distributed way. With this distributed algorithm, a distributed CPPT scheme is designed. To support proper operation of CPPT, the communication network is designed based on a hierarchical wireless mesh network (WMN). Two layer-2 routing protocols are developed to minimize message delivery time: 1) a directional unicast flooding protocol for sending downstream messages; 2) a directional multi-path routing protocol for forwarding upstream messages. All systems involved in CPPT, i.e., the distribution grid, loads, PV systems, and the WMN, are simulated in this paper. Performance results demonstrate the following advantages of CPPT: 1) Voltage in the entire grid is maintained within rating; 2) The amount of reverse power flow stays below a threshold; 3) Surplus power is shared among PV users in a fair manner, as measured by the Jain's fairness index [3]; 4) The performance of the distributed CPPT scheme deviates from the optimal result by only a few percent; 5) Our network protocol guarantees proper operation of the distributed CPPT scheme.

There exist research work related to this paper. Power curtailment in [4], [5] is a local method in regulating voltage, which does not need a communication network or knowledge of grid topology, as an inverter simply reduces output power of a PV system once over-voltage is detected. However, neither the reverse power flow nor fairness problem is considered in a local power curtailment method. The droop-controlled inverters in [6]–[8] can achieve both voltage regulation and proportional power sharing, but the reverse power flow problem is not considered either. The theoretical work in [9], [10] provide distributed solutions to optimal power flow, which can be utilized to control the reverse power flow. However, how to apply these schemes to a practical system remains an open problem. Furthermore, both droop-controlled inverters and the schemes of distributed optimal power flow need admittance matrix of the distribution grid, which is difficult to obtain in practice.

Besides the distributed schemes, many centralized schemes have also been proposed in the literature. In [11], [12], an OLTC-based method is proposed to maximize the reverse power flow by adjusting the tap position of on-load changer transformer (OLTC) so that energy generated by PV systems can be maximally utilized. The over-voltage and fairness problems are addressed in [13], where energy storage system is utilized to store surplus power so that the power generation efficiency among all users is equal. In all these centralized schemes, the reverse power capacity of transformers [14] is neglected.

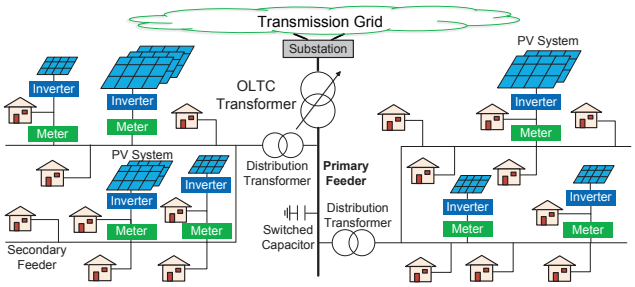

Fig. 1. A distribution grid with PV systems

Compared with the related work, our paper is distinct with the following contributions:

- A complete framework is developed to conduct CPPT for distributed PV systems connected to a distribution grid.
- The mechanism of CPPT is formulated as an optimization problem that maximizes total output power of PV systems subject to the constraints of voltage range, reverse power limit, and fairness. Based on this optimization problem, the conditions of the optimal power points are derived.
- A distributed power point tracking scheme is designed following a weighted max-min fair share algorithm. Based on this scheme and the conditions of the optimal power points, a practical and distributed procedure is developed for CPPT. Abnormal voltage or reverse power flow is also properly handled by the procedure.
- A wireless mesh network is designed to ensure proper operation of CPPT.

The rest of the paper is organized as follows. In Section II the system architecture of CPPT is presented. The optimization problem that determines power points of PV systems is formulated in Section III. A practical distributed scheme is developed in Section IV to track power points of all PV systems The WMN for CPPT is designed in Section V. Simulations and performance results are reported in Section VI. The paper is concluded in Section VII.

II. The Distribution Grid with PV Systems: MPPT versus CPPT

Usually multiple primary feeders are connected to the substation in a distribution grid. However, these primary feeders run independently. Thus, without loss of generality, only one primary feeder is considered in the distribution grid, as shown in Fig. 1. The primary feeder is connected to multiple transformers, each of which supports multiple secondary feeders. Through a secondary feeder, a number of users distributed at different locations are connected to the grid. A user may install a PV system that is connected to the grid through an inverter. For a user with a PV system, we assume there exists a smart meter that can measure power usage and voltage of the user.

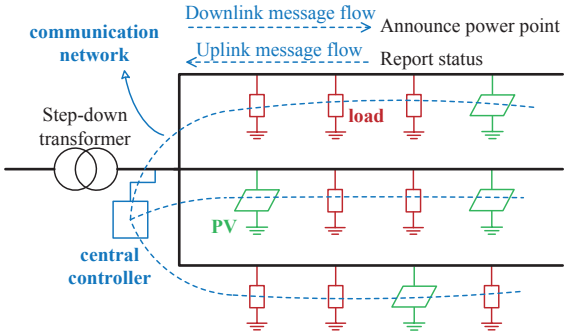

Fig. 2. Major CPPT components in the sub-grid

The smart meter can communicate with the inverter to share its measured information via a communication link such as RS-485. To store surplus power for a PV system, a user may have a battery. Suppose the battery is always enough to absorb the surplus power from a PV system, then the PV system works locally and has no interaction with the grid. In this paper, we consider PV systems that send surplus power to the grid. In other words, we assume no battery is installed or the battery is not enough to store all surplus energy of a PV system. In fact, our assumption is reasonable, because using battery to absorb all surplus power from a PV system demands a large capacity of battery bank, which is expensive in practice. Under our assumption, the battery of a user is considered as part of the load.

Usually output power of a PV system is controlled by an MPPT mechanism in the inverter. However, MPPT results in a few issues. Firstly, over-voltage is not controlled pro-actively. We know that multiple PV systems may make contributions to over-voltage at the same point of the secondary feeders. If the power points of these PV systems are determined in an coordinated way, then over-voltage will occur with a much lower probability. Secondly, the power that flows back to the primary feeder is not controlled. In theory, the reverse operation is doable, but is subject to two constraints: 1) the input voltage level of step-up operation must be controlled strictly within rating to ensure a safe voltage level at the output side; 2) the reverse power flow needs to be controlled so that it does not damage the transformer. As a result, a threshold must be set for the reverse power flow, and the voltage levels at both sides of the transformer must be maintained within rating. Thirdly, the surplus power that can be sent to the grid is not coordinated among different PV systems. Thus, PV systems get unfair share of revenues generated from solar energy. To avoid unfairness, the surplus power allowed in a grid must be fairly allocated to each PV system.

To avoid issues in MPPT, output power control of different PV systems needs to be coordinated. Thus, the focus of this paper is to develop a framework of coordinated power point tracking (CPPT) for grid-connected PV systems. It should be noted that a sub-grid consisting of one transformer and several secondary feeders works independently from another sub-grid. Thus, in this paper, CPPT is studied for a sub-grid instead of the entire distribution grid.

The system architecture that shows the basic operation of CPPT is shown in Fig. 2. CPPT demands a central controller to coordinate the power points of all the PV systems. It is co-located with the transformer where a smart meter is also added to work together with the central controller. The central controller needs to communicate with all PV systems, so a communication network is needed between the central controller and all PV systems. The communication device is usually co-located with the inverter. Through the communication network, an inverter sends status information (e.g., voltage and power of a user) measured by the smart meter to the central controller. The central controller determines the power point of each PV system and then sends such information back. How to determine output power of each PV system will be studied in Sections III and IV. Once an inverter receives a power point, it executes a power point tracking algorithm to track the output power, and the same power tracking algorithm as that in MPPT can be employed. Since the power point is known to the tracking algorithm, the tracking process converges much faster than the entire process of MPPT. As shown in Fig. 2, the central controller and the inverters are connected via a WMN. The reason for using WMN and the design of WMN are addressed in details in Section V.

III. Optimal CPPT

An optimization problem is formulated to determine the power point of each PV system in a distribution sub-grid.

A. Problem Formulation

Connecting points of users and the transformer in the sub-grid are indexed as follows. The connecting point at the secondary side of the step-down transformer is indexed by 0. The connecting point between a secondary feeder and a user with PV system is indexed from 1 to n. Thus, the set of users with a PV system is $\mathcal{N}_1 = \{1, \ldots, n\}$. For users without a PV system, their points connecting with the secondary feeder are indexed by the set of $\mathcal{N}_2 = \{n+1, \ldots, m\}$. Thus, the set of all connecting points in the sub-grid is $\mathcal{N} = \{0\} \bigcup \mathcal{N}_1 \bigcup \mathcal{N}_2 = \{0, 1, \ldots, m\}$. The admittance between i and j is denoted by y_{ij}, so $\mathbf{Y} = [y_{ij}]_{i,j \in \mathcal{N}}$ is the admittance matrix of the entire sub-grid. Let $\mathbf{V} = [V_0, \ldots, V_m]$ be the voltage vector of all connecting points, where $V_i = |V_i| \angle \theta_i$ and θ_i is the phase angle. For a point $i \in \mathcal{N} \backslash \{0\}$, complex power is $S_i = P_i + jQ_i = P_{G_i} - P_{L_i} + j(Q_{G_i} - Q_{L_i})$, where P_{G_i} and Q_{G_i} are the active and reactive power from a PV system, and P_{L_i} and Q_{L_i} are the active and reactive power of load. Currently, a standard PV system only generates active power, so $Q_{G_i} = 0$. For a user without a PV system, both P_{G_i} and Q_{G_i} are zero. Thus, if $P_i > 0$, we know that a PV system i is injecting power to the sub-grid, so P_i is called the *surplus power*.

1) Objective Function: When the output power of all PV systems is maximized, the power pulled from the grid is minimized. Thus, the objective of the optimization problem is to determine the power points of all PV systems such that the power from the grid is minimized. Since only active power is generated in PV systems, the power from grid to

be minimized is also active power. As a result, we have the following objective function:

$$\min_{\{\mathbf{P}_G\}} \quad P_0 \tag{1}$$

where P_0 is the power pulled from the gird and $\mathbf{P}_G = [P_{G_1}, \ldots, P_{G_n}]$ is the vector of powers generated by the n PV systems in the sub-grid.

The variables in the objective function need to satisfy the power flow equation of the sub-grid. Moreover, the objective function needs to consider constraints of voltage, reverse power flow, and fairness.

2) Power Flow Equation: Based on the Kirchhoff law, the power flow equation of the sub-grid can be written as

$$e_i^* \mathbf{V}\mathbf{V}^* \mathbf{Y}^* e_i = S_i, \ \ \forall i \in \mathcal{N}, \tag{2}$$

where $\{e_i\}_{i\in\mathcal{N}}$ is the standard basis vectors in $\mathbb{R}^{|\mathcal{N}|}$, i.e., it is column vector with all zeros except that the i-th element is 1.

3) Voltage Constraint: To ensure proper operation of the sub-grid, voltages of all users need to be maintained within rating. Given the voltage rating $[V_{\min}, V_{\max}]$, the voltage at each connecting point (except for the transformer side) is constrained as

$$V_{\min} + \Delta_V^{lb} \le |V_i| \le V_{\max} - \Delta_V^{ub}, \ \ \forall i \in \mathcal{N}\backslash\{0\}, \tag{3}$$

where Δ_V^{lb} and Δ_V^{ub} are a small value to keep $|V_i|$ from actually reaching the lower limit $V_{\min}$ and the upper limit $V_{\max}$.

Since the step-down transformer is connected to grid, so its voltage is assumed to be fixed, i.e.,

$$|V_0| = V_0^{ref}. \tag{4}$$

4) Reverse Power Flow Constraint: The constraint on the reverse power flow serves two purposes. One is to prevent the step-down transformer from being overloaded. The other is to provide a flexible fine-tuning mechanism for the grid company to control the amount of power flow from distributed generators (e.g., PV systems). The constraints can be applied to both active and reactive power. However, in this paper all PV systems only generate active power, so the reverse power flow can only be active power. Thus, the constraint of reverse power flow only applies to the active power. As a result, we have the following constraint:

$$P_0 \ge P_0^{lb}, \tag{5}$$

where P_0^{lb} is the lower bound for the power flow from grid, i.e., P_0. Since the constraint is for reverse power flow, $P_0^{lb} \le 0$. To protect the transformer, P_0^{lb} must be set to a value much smaller than the power rating of the transformer.

5) Fairness constraint: The surplus power that can be generated by a PV system determines the revenue from this PV system. However, the total surplus power that can be supported by the sub-grid is limited due to constraints of voltage and reverse power flow. Thus, the surplus power must be shared by different PV systems in a fair way. In this paper, we consider a fair allocation strategy according to the size of PV systems. More specifically, the share of surplus power (i.e., P_i) is proportional to the size of the PV panel. In other words, $P_i = k_i c$, where k_i is the size ratio of i-th PV system over all PV systems, and c is the total surplus power. Thus, if a PV system has a larger PV panel, it is allocated with a larger share of surplus power. This strategy is reasonable, because a user with a larger investment potentially receives a higher revenue. Suppose a user's load is P_{L_i} and the maximum output power of its PV system is $P_{G_i}^{\max}$, then the surplus power allocated to this user is limited by $P_{G_i}^{\max} - P_{L_i}$. As a result, the fairness constraint is

$$P_i = \min(P_{G_i}^{\max} - P_{L_i}, k_i c), \ \ \forall i \in \mathcal{N}_1, \tag{6}$$

$$c \ge 0. \tag{7}$$

B. The Optimal Solution and Its Limitations

Without constraints (6) and (7), the optimization problem is non-convex, which is similar to the optimal flow problem in [15]. The additional constraints in (6) and (7) change the non-convex feasible set into a convex one so that the optimal solution can be obtained. Unfortunately, the optimal solution cannot be readily applied to CPPT, for the following reasons:

- The admittance matrix of the entire sub-grid, i.e., $\mathbf{Y}$ is needed, but in fact it is unknown.
- The maximum output power of a PV system, i.e., $P_{G_i}^{\max}$, is unknown, as it depends on the instantaneous operation environment.

However, studying the optimization problem can help us find the conditions under which the optimal solution is achieved. Based on these conditions, we can develop a distributed algorithm to determine the power points of all PV systems.

C. Conditions on Optimal Power Points

In this section, we first prove several lemmas and then derive the theorem for the optimal conditions.

Lemma 1. *If the voltage constraint in Eq. (3) is satisfied, then PV systems get their optimal power points either when the reverse power constraint in Eq. (5) is reached or when all PV systems generate maximum output power.*

Proof: The proof is provided in Appendix A. ■

Lemma 2. *If the voltage at any point $i \in \mathcal{N}\backslash\{0\}$ reaches its upper bound (i.e., $V_{\max} - \Delta_V^{ub}$), then no PV system can increase output power.*

Proof: The proof is provided in Appendix B. ■

Theorem 1. *Maximum power allocation is achieved at all PV systems under any of the following three conditions: 1) Voltage upper bound is reached; 2) Reverse power flow reaches the threshold; 3) The maximum power points of all PV systems are reached.*

Proof: Considering condition 1), when any voltage reaches the upper bound, Lemma 1 shows that all PV systems have to stop increasing output power, i.e., maximum output power is achieved at all PV systems. From Lemma 1, when voltage upper bound is not reached, we can always increase output power of a PV system till condition 2) or 3) is satisfied. As a result, optimal power points of PV systems are achieved under any of conditions 1), 2) and 3). ■

IV. Coordinated Power Point Tracking Via a Communication Network

Based on the conditions of optimal power allocation in Theorem 1, a practical approach to distributed CPPT is developed in this section.

A. Basic Mechanisms of Distributed CPPT

As shown in Fig. 2, the central controller and inverters of PV systems work collaboratively via a communication network. The distributed CPPT includes the following major mechanisms: 1) Inverters collect local information for the central controller, and the central controller determines power points accordingly; 2) PV systems track output power according to the allocated power points; 3) CPPT is executed for multiple rounds until conditions on optimal power points are reached. As proved in Theorem 1, there exist three conditions under which PV systems have achieved the maximum allowed power points. Two conditions (i.e., conditions 1) and 3)) have to be checked locally by a PV system, while one condition (i.e., condition 2) needs to be checked at the central controller. The communication network plays an important role. Via this network, the distributed CPPT scheme works like a networked controlled system.

B. Surplus Power Allocation Algorithm

As shown in the fairness constraint of the optimization problem in Section III, PV systems can just share surplus power according to their PV sizes. However, the allocated power share may not be achievable by a PV system, because of three other constraints: 1) over-voltage constraint; 2) reverse power flow constraint; 3) maximum output power of a PV system. Thus, a surplus power allocation algorithm is needed.

In CPPT, surplus power allocation can be viewed in two perspectives. From the perspective of the central controller, surplus power allocation is simply a proportional fair share algorithm. Given a PV system i, its smart meter reports the surplus power, i.e, $P_{S_i} = P_{G_i} - P_{L_i} \geq 0$. Suppose total number of PV systems is n, then the total surplus power from all PV systems is $\sum_{i=1}^{n} P_{S_i}$. Suppose currently the active power drawn from the transformer is P_0 and the allowed reverse power is P_0^{lb}, then the surplus power that can be allocated to PV systems is $P_S = P_0 - P_0^{lb} + \sum_{i=1}^{n}(P_{G_i} - P_{L_i})$. This means that PV systems are allowed to generate output power as much as what can be sent to the grid (i.e., either consumed by loads or sent to the grid via the transformer). Thus, P_S is actually the parameter c in the fairness constraint in Eq. (6). Since the central controller knows the ratio of PV size between different PV systems, i.e, the parameter k_i in Eq. (6), the new surplus power P_i allocated to PV system i is $P_i = k_i P_S$. As a result, the new power point (the output power) of PV system i is $P_{G_i} = P_i + P_{L_i}$.

When the new power point is sent from the central controller to a PV system, the inverter tracks the new power point accordingly. However, it is highly possible that such a new power point is not achievable due to three constraints as mentioned before. Thus, the PV system can only generate an output power smaller than the allocated value. In this case, another round of power allocation is needed so that the above proportional fair share algorithm is executed again to allocate the unused surplus power. After a few rounds, all surplus power is allocated, and the entire CPPT algorithm converges. Thus, from the perspective of the entire CPPT algorithm, power allocation is actually a weighted max-min fair share algorithm [2]. More specifically, the weight is k_i, and the demand of max-min fair share for each PV system is the limit of surplus power that is allowed by the PV system. Consequently, our distributed CPPT algorithm can achieve graceful fairness. The fairness performance will be evaluated through Jain index in Section VI.

C. Procedures and Messages Involved in CPPT

The operation procedures of the distributed CPPT scheme are explained as follows.

- Once a PV system starts to work (e.g., in the morning as the sun rises), its inverter controls output power to track the local load. It then reports its status to the central controller via the communication network periodically, e.g., 5 seconds.
- When the central controller receives status information from all PV systems, it determines a new power point for each PV system based on the algorithm explained in Section IV-B. The new power point is then sent back to each PV system via the communication network.
- Once a PV system receives the new power point, it executes the local power tracking scheme to update its output power. Local power tracking may lead to three different results. First, the new power point is properly reached. Second, output power is already maximum before reaching the new power point. In both cases, the inverter just sends back the new status information to the central controller. Third, over-voltage occurs during local tracking. In this case, the inverter invokes voltage curtailment to reduce output power, i.e., it reduces output power to track the local load only. Once voltage curtailment is done, the new status information is reported to the central controller.
- Once the central controller receives the new status information from PV systems, it checks if any of the three optimal conditions is reached. If so, the central controller sends the current power points of PV systems to inverters indicating that CPPT has converged. The central controller also constantly monitor the reverse power flow. Once the reverse power flow reaches the threshold, the central controller immediately determines new power points and then send such information to all PV systems. If this event occurs during a new round of power allocation, the new power points just overwrites the previous allocated power points.

The above procedures repeat constantly so that all PV systems are adaptive to dynamic system parameters such as variable loads and PV output power.

In the operation procedures of CPPT, three types of messages are exchanged between CPPT and inverters. Message

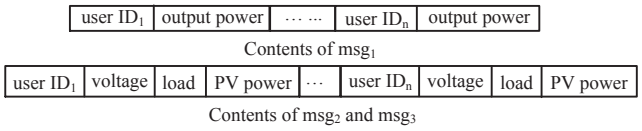

Fig. 3. Contents of different messages

type 1 (msg_1) is sent from the central controller to an inverter, and is thus a *downstream message*. This message is generated whenever power point information is announced to inverters. However, for the purpose of reliable delivery, a message must be confirmed to be received by an inverter. Thus, msg_1 needs to be sent to inverters following a one-to-many unicasting scheme. The frequency of sending msg_1 is determined by the times of power tracking till convergence of CPPT. The contents of msg_1 are shown in Fig. 3, where n is the number of inverters.

Message type 2 (msg_2) and message type 3 (msg_3) are sent from an inverter to the central controller to report status of a PV system, so they are called *upstream messages*. msg_2 and msg_3 have the same contents including ID, PV output power, voltage, and load as shown in Fig. 3, but they are generated at different times. msg_2 is sent by an inverter to the central controller right after local power tracking is done, while msg_3 is sent periodically from an inverter to the central controller. Thus, the frequency of msg_2 is determined by the times of power tracking till convergence of CPPT, while the frequency of msg_3 is determined by a period T_p. When msg_2 is triggered during a certain period, then msg_3 in this period is revoked.

The timing relationship of the above three types of messages is shown in Fig. 4. The network delay of each message type means the total delay for all the same-type messages to be received reliably. QoS requirements of three types of messages are two-fold. For each individual message, it must be delivered reliably. Since packet loss probability is nonzero in a wireless network, retransmission is needed. For each type of message, another requirement is that the entire group of messages must be delivered within a delay limit. We denote the delay limits for msg_1, msg_2, msg_3 as D_1, D_2, D_3, respectively. We know that D_1 and D_2 impact the total communication time for one round of power point tracking in CPPT. Thus, to ensure fast convergence of CPPT, D_1 and D_2 need to be minimized. D_3 does not impact convergence time of CPPT, but determines the response time of collecting status of the grid. Thus, delay requirement on D_3 is not as critical as that on D_1 or D_2, but minimizing D_3 is still expected for fast response to changing status of the grid. In Section V-B, protocols will be designed to minimize D_1, D_2, D_3. The special case handling of missing messages is also discussed in Section V-B.

D. Functions at the Central Controller

Several functions are implemented in the central controller. The first function is to allocate appropriate power points for PV systems according to the algorithm in Section IV-B. To this end, the central controller needs to collect status information (e.g., load, current output power, voltage) of each PV system. The status information also helps the central controller to determine if CPPT has converged. The second function is to monitor reverse power flow of the transformer via a smart meter. Once the reverse power flow exceeds the threshold, the central controller immediately recalculate the new power points, and then inform PV systems of this new power allocation. The third function is a communication module supporting the communication network.

E. Functions at a PV System

As explained in Section II, the functions of CPPT at the PV side involve several devices including a smart meter, an inverter, and a communication module co-located with the inverter. Based on these devices, the PV side needs to conduct three functions for CPPT: 1) communicate with the central controller through the network; 2) collect the status information (e.g., load and PV output power) and report it to the central controller; 3) track power point of PV according to the allocated power; 4) monitor the voltage and perform voltage curtailment when over-voltage occurs. The first function will be explained in detail in Section V, and the second function is straightforward. The local power tracking scheme has no difference from other power point tracking algorithms (e.g., MPPT), as explained in Section II. Thus, in this subsection only the fourth function and its property are addressed in details.

1) Voltage Curtailment at a PV System: In CPPT, power points are determined based on the status information reported from PV systems. However, due to network delay, loads of users may have changed before the distributed CPPT scheme finishes power tracking for all PV systems. If loads are dropped significantly, then the surplus power allocated to PV systems may result in over-voltage. Voltage curtailment is needed to respond to over-voltage. It is carried out by the inverter of a PV system. Once over-voltage is detected by the smart meter, the inverter immediately drops its power point to track the local load (as measured by the smart meter). This approach can quickly stop power flow to the grid, and thus can effectively pull the voltage back to normal.

2) Effectiveness of Voltage Curtailment: The following theorem states that voltage curtailment is effective.

Theorem 2. *The voltage curtailment scheme can resolve the over-voltage issue at all users (including those without PV systems) within one round of local power tracking.*

Proof: Over-voltage may occur in two cases.

Case 1*: Over-voltage happens at user i, but voltages at its neighbors are normal.* In this case, user i must have a PV system, because power flows from a higher voltage to a lower one. In response to over-voltage, the inverter for the PV system applies voltage curtailment by tracking the local load. After a delay of local power tracking, no active power will flow from user i to neighbors. Thus, the direction of power flow between users i and its neighbors is changed, and the voltage of user i must be lower than upstream neighbors and higher than downstream neighbors. Since these neighbors have a normal voltage level, the voltage at user i is now back to normal. As shown in Fig. 5, user 2 has a PV system and experiences

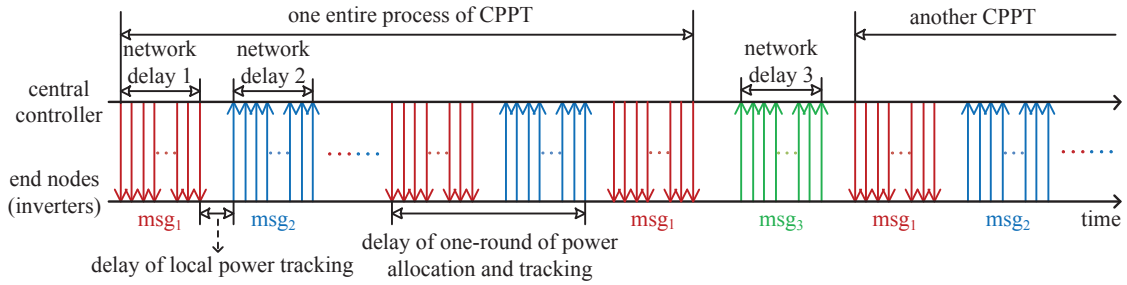

Fig. 4. Timing relationship of messages between the central controller and inverters

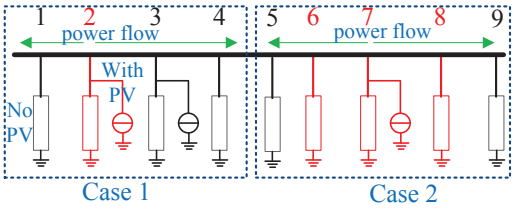

Fig. 5. Illustration of two over-voltage cases

over-voltage. After it has done voltage curtailment, the power will flow either from user 3 to 1 or the opposite, and thus user 2 has a normal voltage. This recovery process only takes the time of local power tracking, so it is completed within one round of power tracking.

Case 2: Over-voltage occurs at user i and also its neighbors, but other nearby users have normal voltage. If a user with no PV system has over-voltage, then some neighbors with the same over-voltage issue must have a PV system. Such neighbors with PV apply the voltage curtailment scheme, and then power flow is then changed. As shown in Fig. 5, users 6 and 8 have no PV but experience over-voltage, user 7 with a PV system has the same over-voltage issue, and other users have normal voltage. After the inverter of user 7 finishes local power tracking, power will flow either from user 5 to 9 or vice versa. No matter what direction of the power flow, users 6, 7, or 8 recover their voltage to normal, since both user 5 and 9 have normal voltage. Thus, the over-voltage issue of case 2 can be resolved within one round of local power tracking. ■

F. Convergence of CPPT

The convergence of the distributed CPPT scheme is impacted by two major factors. Firstly, power loss and users' loads change from time to time. Thus, if the change occurs before CPPT converges, then a new set of power points are needed for PV systems. If the communication network and the local power point tracking scheme are fast enough, then CPPT can always converge. Secondly, the allocated power point may not be reached due to three constraints, i.e, voltage, reverse power flow, and maximum output power. Thus, new power point needs to be adjusted in another round of CPPT. The number of rounds depends on the settings of the sub-grid, but as shown in Section VI, usually 3-4 rounds are sufficient to converge. To avoid performance degradation due to multiple rounds of power allocation, the total delay for one round of allocation needs to be as small as possible. Considering the above two factors, the convergence of CPPT is closely related to performance of the communication network. In Section V, the design goal of the communication network is to minimize the message delivery delay. Impact of the designed network to CPPT performance is evaluated in Section VI.

V. Network Design for CPPT

CPPT is supported by a communication network between the central controller and inverters. Convergence of the distributed algorithm in CPPT depends on timely delivery of messages between the central controller and all inverters. More specifically, the smaller the message delivery time is, the faster CPPT converges. Thus, the design goal of the communication network for CPPT to minimize the message delivery time.

To achieve this goal, a communication network can be designed based on either wired or wireless network. Although optical networks are commonly deployed for distribution grid and substations, they are not readily available in distribution grid. Deploying a dedicated wired network (including power line communication network) for CPPT is a costly option. If public wired networks, such as the Internet connection, are used to carry traffic of CPPT, then it is necessary to request the service provider to guarantee QoS for CPPT, which is not an economical and feasible approach. As a result, wireless networks become a more viable option.

To cover an area (usually a few square kilometers or more) of a distribution grid, both cellular networks and wireless mesh networks (WMNs) can be adopted. However, we do not consider cellular networks in this paper for two reasons: 1) Frequent message exchange in CPPT results in high usage of cellular networks, which is too expensive; 2) A low rate cellular link results in high message delivery time, but a high rate cellular link is costly. Moreover, carrying CPPT messages through a cellular network has the same problem as that of a public wired network. Thus, the better choice for CPPT is WMN. In what follows, we focus on the design of a WMN such that proper operation of CPPT is ensured.

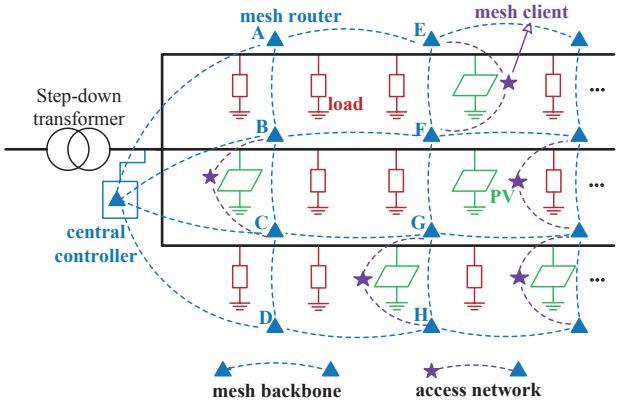

Fig. 6. Two-layer hierarchical WMN for CPPT

A. Mesh Network Architecture for CPPT

Naturally the mesh network for CPPT consists of two hierarchy. The upper hierarchy consists of mesh routers that work in the same frequency channel and are connected like a multi-hop mesh network. It provides a wireless backbone to carry traffic between end nodes and the central controller. The lower hierarchy consists of access networks for end nodes (i.e., communication modules in inverters). A mesh router bridges an access network and the mesh backbone.

To avoid interference, the two hierarchies work in different frequency band, and neighboring access networks work in orthogonal frequency channels. In theory, one radio is sufficient to support all functions of a mesh router. However, to make protocol design simple, dual radio is considered, i.e., one radio for mesh backbone and the other for network access by end nodes.

1) Hierarchical Mesh Network Architecture: The two-layer hierarchical WMN is depicted in Fig. 6, where the topology of a distribution sub-grid is also shown. The WMN takes reliability as a critical design factor. As a result, each branch of secondary feeders is covered by two different sets of mesh routers. As shown in Fig. 6, there are 4 sets of mesh routers deployed along three branches of the secondary feeders. As a result, the central controller is connected to 4 mesh routers, and each end node can be connected to two mesh routers.

2) WiFi Mesh versus Zigbee Mesh: To build the hierarchical WMN for CPPT, there exist two major options: WiFi mesh or Zigbee mesh. In this paper, WiFi mesh is selected by considering the following factors:

- The communication nodes are not constrained by battery life, as they are co-located with power devices. Thus, Zigbee is not required.
- Considering a distribution sub-grid in a residential area, the communication distance between routers is usually in a range of about 100 meters. The distance between a mesh router and an end node is shorter than 100 meters. Thus, we do not need to rely on Zigbee to achieve long communication range.
- The raw data rate of Zigbee is only 20-250 Kbps, which is much lower than the 6 Mbps data rate of WiFi even if 1/2 BPSK is used. Since delay is critical to CPPT performance, so WiFi is a safer choice.

Although WiFi mesh is selected for CPPT, we do not conclude that Zigbee is infeasible for CPPT. How to make Zigbee work for CPPT is subject to future research. It should be noted that only a few end nodes are covered by a mesh router, so the new IEEE 802.11 protocol being developed for smart grid, i.e., IEEE 802.11ah [16], is not necessarily needed for CPPT.

B. Protocol Design

To ensure the CPPT algorithm converges fast and reliably, the communication delay in one round of CPPT must be minimized, subject to the constraint of link quality and network topology. To this end, we need to minimize the end-to-end delay of a message and also the number of messages involved in CPPT. To achieve this goal, a few design rules are followed:

- The timing relationship between different messages must be explored. In CPPT upstream messages and downstream messages are logically separated. Thus, message delivery protocols for downstream and upstream can be conducted separately for the benefit of a higher time efficiency.
- Different messages to the same destination need to be consolidated. The rationale behind this strategy is that the content of each message is small; fusing these messages can significantly reduce message delivery delay. For example, in the upstream, messages from different end nodes can be merged at their associated mesh router and then forwarded to the central controller through the mesh backbone.
- Protocols are designed specifically for the proper operation of CPPT. Thus, a complete protocol stack must be avoided. In fact, a protocol needs to be designed as simple as possible.

Considering the above design rules, we propose a *layer-2* message delivery protocol for CPPT. In this protocol, there is no transport or network layer; instead, CPPT messages are carried directly through a layer-2 protocol. Moreover, the layer-2 protocol runs separately for upstream and downstream messages.

1) Protocol for Downstream Messages: Since each inverter needs to get a power point, message delivery from the central controller to all inverters is a one-to-many unicast problem. Unicast is required for reliable delivery, but one-to-many unicast results in large overhead and delay, if a conventional protocol stack like TCP/IP is followed. To avoid large delay and overhead, a layer-2 downstream protocol is design in this section.

With a layer-2 protocol, when a message is delivered to an end node, it needs to be carried hop-by-hop through the WMN till reaching the end node. However, a layer-2 routing is needed. Moreover, if all end nodes need to receive a message from the central controller, then the delay is high. To resolve these issues, two mechanisms are designed: i) power point information to all PV systems is consolidated in one message, and the central controller only needs to initiate one message for all end nodes; ii) a directional flooding scheme is used in layer 2, so that the message from the central controller can be sent hop-by-hop to all mesh routers and their associated

end nodes. Since reliability is critical, so the flooding actually conducts unicasting and requires ARQ. Thus, the directional flooding protocol is a *directional unicast flooding scheme*.

With the above ideas in mind, the downstream protocol works as follows:

i) Once the central controlled has determined power points for all PV systems, such information is consolidated into one downstream message, i.e., msg_1.
ii) The message is embedded into a layer-2 packet, and then sent to all neighboring mesh routers, e.g., A, B, C, D in Fig. 6, in a round-robin style. Once a mesh router, e.g., A, has received the message, it carries out two tasks. One is to flood the messages to all of its associated end nodes. The other is to forward the message to all of its neighboring routers except for the router that the message is received from. In this case, A forwards the message to B and E. However, when B receives the message, it discards it and knows that forwarding a message to A is not necessary.
iii) Step ii) is repeated until all end nodes receive the message.

The layer-2 directional unicast flooding scheme is featured by several advantages: i) It matches the characteristics of downstream messages in CPPT; by nature delivering one message to all end nodes is a flooding process; ii) It eliminates transport layer reliability, and thus significantly reduces the end-to-end delay; iii) Routing is performed in layer 2 via a flooding process; iv) It is directional flooding, since a message always flows downstream to end nodes; v) Reliability is high, because flooding takes advantages of all links.

2) Protocol for Upstream Messages: Similar to the downstream protocol, the upstream protocol is designed as a layer-2 protocol. However, since messages are initiated from different end nodes and then carried by the mesh backbone to the central controller, this process is much different from a flooding process. Thus, a different layer-2 routing protocol is needed to forward a message all the way to the central controller.

The upstream protocol consists of three major mechanisms: i) message delivery from an end node to a mesh router ii) message fusion at mesh routers; iii) message forwarding through the mesh backbone to the central controller. The second mechanism is necessary to reduce traffic load from small messages, but it is simple; as a mesh router receives all messages of its associated end nodes, it consolidates these messages into one message. The details of the first and the third mechanisms are explained below.

a) Message delivery from an end node to a mesh router: An end node can be associated with more than one mesh routers. All these mesh routers are considered as candidate routers to receive messages from the end node, but only one is selected based on a criterion such as the best link quality. The procedure of maintaining candidate mesh routers and selecting the best one is done in the background as part of the link management protocol. Once a mesh router is selected by an end node, it is informed of this selection via the link management protocol. Thus, a mesh router always knows how many end nodes are associated with it. Moreover, when a message (either msg_2 or msg_3) is initiated at an end node, it is sent to a specific mesh router.

There are two scenarios of upstream messages: msg_2 and msg_3. For msg_2, since it is initiated by an end node only upon the end of local power tracking, messages of msg_2 do not suffer from collisions due to concurrent transmissions. However, msg_3 is initiated periodically by end nodes. As explained in V-B3, proper operation of CPPT requires synchronization among end nodes. Thus, messages of msg_3 from different end nodes can easily collide due to concurrent transmissions at the beginning of each period. To avoid this issue, each end node starts an random backoff at the beginning of a period before sending msg_3. This backoff is different from that in CSMA/CA. Usually CSMA/CA does not conduct backoff when a channel is clear and the backoff counter is zero.

b) Message forwarding in the mesh backbone: A layer-2 routing protocol is designed to forward a message from a mesh router to the central controller. Similar to the first mechanism, each mesh router maintains a list of candidate mesh routers for message forwarding, but only one is selected for actual forwarding based on a criterion. Different from the first mechanism, two metrics are considered together as a criterion for selecting a mesh router: the link quality and the minimum hop to the central controller. Instead of choosing a mesh router with the best link quality, we select a mesh router that has a minimum-hop path to the central controller. However, the link quality along this path must be satisfactory; otherwise, the next candidate path is considered. Following the afore-mentioned process, each mesh router in the mesh backbone selects a mesh router as its next hop. As a result, once a message is received, it can be easily forwarded to the next hop till the central controller.

Our upstream layer-2 routing protocol are characterized by several features: i) *directional forwarding*, i.e., it selects the next-hop mesh router in the upstream to forward a message; ii) *multi-path routing*, because candidate routing paths are maintained; iii) *efficient forwarding*, i.e., messages are consolidated to reduce unnecessary overhead and delay. As a result, our layer-2 routing protocol is actually an efficient *directional multi-path layer-2 routing protocol*.

3) Link Management Protocol: To support layer-2 protocols for both upstream and downstream messages, several functions need to be added into a link management protocol in the data link layer.

The first function is to determine hop count from a mesh router to the central controller. To do so, each mesh router adds one additional information element, i.e., hop count to the central controller, into its beacon. The central controller always announces a hop-count 1 to all its neighboring mesh routers. For other mesh routers, the initial value of hop-count is infinite, as indicated by a special character. Once a neighboring mesh router gets a beacon from the central controller, its hop count is set to 1, since its next-hop router is the central controller. The neighboring mesh router then announces a hop count 2 in its beacon. When another mesh router receives such a beacon, it compares the new hop count in the beacon with the old hop count. If the new hop count is smaller, then it is updated; otherwise, no change is needed. It should be noted

that each mesh router maintains a hop count (to the central controller) via each of its neighboring mesh routers. Thus, each mesh router in the mesh backbone knows how many hops are needed from each of its neighboring routers to the central controller.

The second function is to maintain candidate mesh routers and select the best for message forwarding. This function is simple, as neighbor list and link quality maintenance are already implemented in an IEEE 802.11 link management protocol. For an end node, it utilizes such link quality information and selects the best one. The additional step is to announce its selected router. This can be done via a beacon or using a unicast management packet. For a mesh router, the next-hop mesh router is simply selected by considering hop counts that are determined in the first function: If a neighboring mesh router has the minimum hop count and its link quality is satisfactory, then it is selected as the next-hop mesh router; otherwise, the next neighboring mesh router is considered.

The third function is to synchronize end nodes. End nodes need to be synchronized, because the central controller expects all end nodes to report grid status information within the same time period. Otherwise, the cental controller has to wait an uncertain timeout window. To synchronize clocks in end nodes, the standard timing synchronization function (TSF) function in IEEE 802.11 is employed. Based on the synchronized TSF, the central controller sends a starting time of periodical reporting messages (i.e., msg_3) as a new element in its beacon. All neighbor mesh routers forward such information in their beacons. Once an end node gets this information from a beacon, it knows when msg_3 can be initiated.

4) Optimization of the Protocol: Our protocol design has explored the specific characteristics of messages in CPPT. It is simple, practical, and effective. However, it is not necessarily optimized. We believe some functions or mechanisms in this protocol can be improved, but complexity will increase too. For example, it is possible to further consolidate upstream messages in the mesh backbone. The efficiency of doing so may be limited, as the messages are already large after consolidation in the access network. Another example is that, when a downstream message has passed a mesh router, all information for the end nodes of this mesh router can be removed. This process reduces overhead, but cause higher complexity. It should be noted that the main purpose of message consolidation in our protocol is reducing network delay instead of overhead.

5) Impact of Link Quality: To ensure reliability of message delivery, an erroneous message needs to be retransmitted. When link quality is low, multiple retransmissions are needed, which results in a large delay. The message delivery delay impacts the delay in reaction to the reverse power flow, as will be demonstrated in Section VI. When link quality degrades further, a node may lose all its available links to its neighbors. As a result, the connection between this node and the central controller is lost. However, such an event can be detected by both the node and the central controller. Based on the timing relations and message flows in Fig. 4, the central controller can find out that its association with an end node is lost either based on msg_2 or msg_3. The central controller knows an end

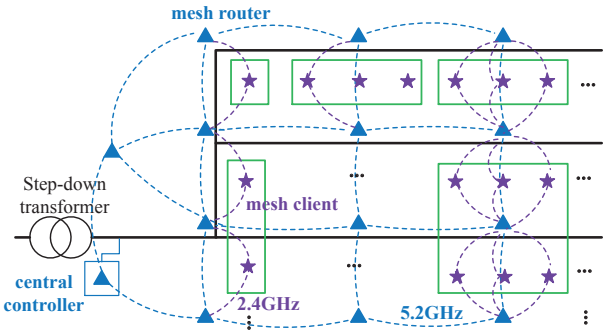

Fig. 7. The communication network topology in experiments

node is lost if it does not receive msg_2 from the end node even after a timeout window expires. The length of the window is equal to the sum of the maximum network delays of msg_1 and msg_2 and the local tracking time. When the central controller does not receive msg_3 from an end node even after period T_p expires, it can also conclude that the end node is lost. Similarly, an end node knows it is isolated from the wireless network if it does not receive msg_1 from the central controller for a period longer than the sum of the maximum network delays of msg_1 and msg_3.

After identifying an isolated end node, the central controller starts a new round of CPPT by excluding this node. For the isolated end node, it simply controls the output power of its PV system to track its local load. In this way, CPPT can still converge quickly after a few rounds, but the power points of PV systems are not optimal and fairness among PV systems is lost. However, since link failure is usually temporary, the time period in which fairness is impacted is negligible as compared to the power generation time of an entire day. In case a link failure is permanent, an isolated node can just simply turn off its PV and signal an alarm for network maintenance.

VI. Performance Evaluation

To evaluate the performance of CPPT, several experiments are conducted through simulations on MATLAB platform. The physical system and the communication network are effectively integrated.

A. Experiment Setup

1) Physical System Setup: A residential 220 V distribution sub-grid is considered with a 100 KVA transformer and 50 users. These users are connected to the transformer via 5 feeders with 10 users on each feeder. The impedance of these feeders is specified as in [17]. The distance between adjacent users is 40 m and the distance between transformer and the nearest user is 150 m. In the network, 50% random selected users are equipped with PV systems. One round of local power tracking time for a PV system is set to 0.01 s as in [18]. The areas of PV systems vary from 10 m^2 to 30 m^2, and the efficiency of each PV system is set to 16.5%, i.e, a 10 m^2 PV system can generate 1.65 KW power if solar radiation is 1 KW/m^2. Hourly solar data in [19] is adopted to simulate the variation of solar radiation. In our experiments, each user

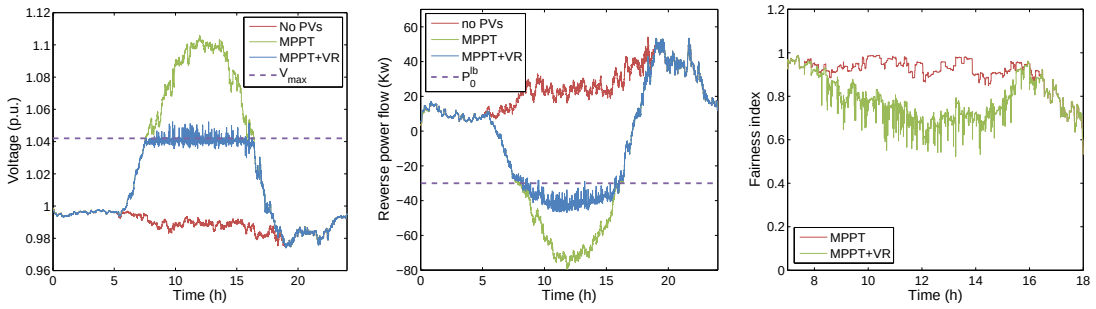

(a) Voltage profile (b) Reverse power flow profile (c) Fairness profile

Fig. 8. Performance of MPPT-based schemes.

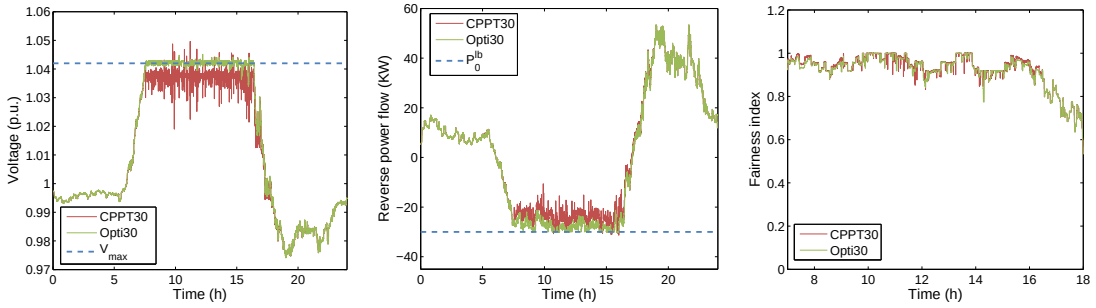

(a) Voltage profile (b) Reverse power profile (c) Fairness profile

Fig. 9. Performance of a CPPT scheme.

has 12 types of appliances with an average power factor of 0.9. 20% of these appliances have rated power between 1 KW and 2 KW, while the rest consume power less than 1 KW. Load change of each user is modeled as a Poisson process with average frequency equal to 7 times/hour.

2) Communication Network Setup: On both sides of the feeders, mesh routers are deployed uniformly so that each user can access at least 2 mesh routers. To mitigate interference, each mesh router is associated with at most 6 users. Moreover, 50 users are divided into 12 groups as in Fig. 7, where only half of the entire topology is illustrated. Users located in one green square belong to the same group and transmit their messages using the same channel on 2.4 GHz band. Adjacent groups adopt different channels. Also, the communications between mesh routers are conducted on a channel in 5.2 GHz band. The bandwidth of theses channels are all equal to 20 MHz.

In addition, the size for each type of message is summarized as follow. msg_1 carries the power allocation information for 25 inverters, each with 6 bytes. This leads to a payload of 150 bytes. msg_2 and msg_3 are generated by inverters and include the system parameters. To carry such information, 15 bytes are required for a msg_2 or msg_3 from an inverter. After the message aggregation at a mesh router, the size of an aggregated msg_2 or msg_3 become 90 bytes at most, since there are at most 6 users associated with a mesh router.

B. Physical system evaluation

To investigate whether MPPT-based schemes can be effectively applied to distribution PV systems, the performance of MPPT and MPPT with voltage regulation (VR) is evaluated under our experiment setup. As shown in Fig. 8, performance results for three metrics are presented: the maximum voltage among all users (Fig. 8(a)), the reverse power flow at the transformer (Fig. 8(b)), and Jain fairness index of surplus power sharing (Fig. 8(c)). The formula for Jain index is $\mathcal{J} = \left(\sum_{i\in S} x_i\right)^2 / (n \sum_{i\in S} x_i^2)$, where S is the set of PV systems that are sending surplus power into grid, n is the number of PV systems in S, and $x_i = \frac{P_i}{k_i}$. From Fig. 8(a), it can be observed that the maximum user voltage always exceeds the safety threshold (i.e., $V_{\max}$) during day time, which is significantly detrimental to the distribution grid. This situation is alleviated when MPPT is combined with VR, which can effectively control user voltage to a reasonable value. However, MPPT with VR has other problems. As shown in Fig. 8(b), the reverse power at the transformer is higher than the maximum tolerable value (i.e., $P_0^{lb} = -30$ KW). Moreover, the Jain index shown in Fig. 8(c) indicates that MPPT with VR incurs serious unfair share of surplus power between different users. The above results confirm that MPPT-based schemes are not effective to a distribution grid with PV cells.

To evaluate CPPT, a CPPT scheme denoted as CPPT30 (where "30" indicates the maximum tolerable reverse power flow in KW) is considered first. In the experiments, the same setup as mentioned in Section VI-A is adopted, and the average round-trip communication delay is 300 ms, which is a conservative value based on results shown in Section VI-D. This round-trip delay contains two parts. The first part is the downlink delay that is required to distribute messages from the central controller to all inverters. The second part is the waiting

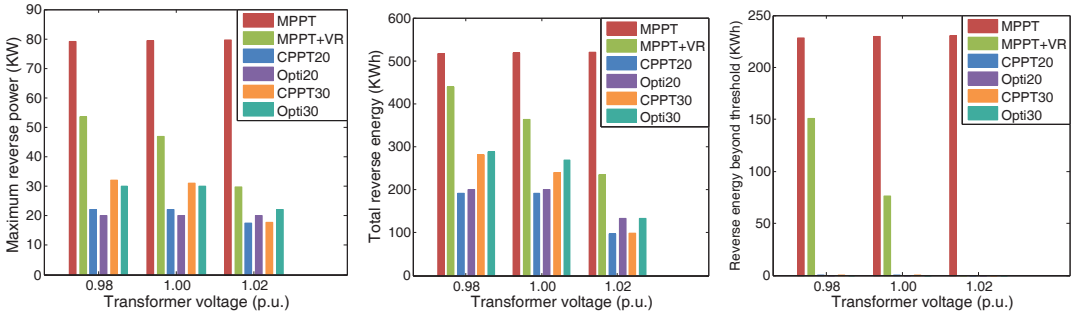

(a) The maximum reverse power (b) Total reverse energy (c) Reverse energy beyond threshold

Fig. 10. Performance of different schemes at different voltages

TABLE I
JAIN INDEX UNDER DIFFERENT TRANSFORMER VOLTAGE LEVELS

Voltage (p.u.)	Jain index			
	MPPT	MPPT+VR	CPPT30	Opti30
0.98	0.990	0.940	0.993	0.993
0.99	0.990	0.920	0.992	0.993
1.00	0.990	0.888	0.993	0.993
1.01	0.990	0.847	0.993	0.993
1.02	0.990	0.795	0.993	0.993
1.03	0.990	0.757	0.992	0.993

TABLE II
OVER-VOLTAGE TIMES AND AVERAGE ROUNDS OF CPPT IN A DAY

Voltage (p.u.)	Over-voltage times		Average rounds for CPPT30
	MPPT+VR	CPPT30	
0.98	167	0	1.2
0.99	245	6	1.3
1.00	330	25	2.9
1.01	398	24	2.9
1.02	416	26	2.8

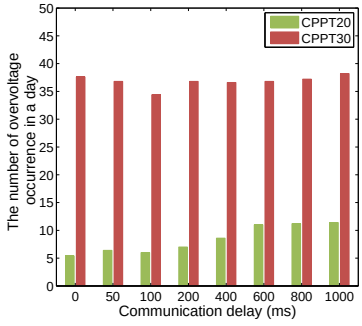

Fig. 11. The number of over-voltage occurrence at different delays

time of the central controller to collect all feedback messages from inverters. The power point tracking time is not included in this delay. For comparison, the performance for CPPT under ideal conditions, i.e., no communication and tracking delay, is also provided (denoted as Opti30). As shown in Fig. 9, the user voltage and the reverse power flow are well controlled with the CPPT scheme and the fairness index is sigificantly improved as compared to that of MPPT-based schemes. For all three performance metrics, the CPPT scheme closely follows the ideal CPPT (i.e., Opti30). The small gap is mainly due to the existence of the voltage margin ΔV^{ub}. All these results demonstrate the effectiveness of our CPPT scheme.

To further evaluate the performance of the CPPT scheme, we investigate three performance metrics under different voltage levels at the transformer. The results are shown in Fig. 10, Table I, and Table II, where the Jain index measures the fairness of surplus energy sharing among PV systems in a day, i.e., $x_i = \frac{E_i}{k_i}$ and E_i is the energy generated by PV system i. As the voltage level at the transformer increases, following results are observed: 1) the reverse power flow reduces; 2) the number of over-voltage occurrence increases; 3) the unfairness of MPPT with VR becomes more severe while that of CPPT remains unchanged. These results are attributed to the fact that users voltages increase as the voltage at the transformer rises. The voltage increase at user side suppresses the power injection from PV into the grid and also makes over-voltage occur more often. Since CPPT includes a mechanism of fine-grained coordination among different inverters, it effectively adapts voltage rise at the transformer, which shows a great advantage over the MPPT-based schemes. This experiment also shows an interesting result (see Table II: the average rounds for CPPT to converge are within 3 times.

C. Relation Between Communication Delay and CPPT Performance

We conduct experiments to evaluate CPPT performance with respect to different round-trip delays. In these experiments, to capture abrupt and significant load variations, we consider an *extreme event* where 10 users with no PV systems pull out their own large appliances (1.5 KW) within 1 s. Thirteen such events are uniformly inserted into the period from 7 a.m. to 7 p.m. Also, Besides CPPT30 as mentioned previously, CPPT20 is also evaluated, where a more tight bound on the maximum reverse power flow, i.e. 20 KW, is imposed.

The variations of three metrics, i.e., times of over-voltage occurrence, Jain fairness index, and reverse power flow, under different round-trip delays are presented in Fig. 11, Table III, and Table IV, respectively. From Fig. 11, it can be observed that the number of over-voltage occurrence in CPPT20 slowly

TABLE III
FOUR PARAMETERS OF THE REVERSE POWER FLOW WITH RESPECT TO ROUND-TRIP DELAY

Delay (ms)	**Max. exceeded power (KW)**		**Exceeded energy (KWh)**		**Max. exceeded time (s)**		**Total exceeded time (s)**	
	CPPT20	CPPT30	CPPT20	CPPT30	CPPT20	CPPT30	CPPT20	CPPT30
0	3.978	1.836	0.097	0.001	0.028	0.024	2.174	0.090
50	5.131	2.216	0.099	0.000	0.219	0.112	10.05	0.348
100	6.245	2.561	0.102	0.001	0.368	0.181	17.93	0.598
200	7.091	2.863	0.106	0.001	0.692	0.298	32.63	0.994
400	9.538	3.482	0.114	0.002	1.455	0.640	59.65	1.848
800	11.86	3.699	0.130	0.002	2.826	1.121	112.9	2.850

TABLE IV
FAIRNESS VERSUS COMMUNICATION DELAY

Delay (ms)	**Jain index**	
	CPPT20	CPPT30
0	0.993	0.991
50	0.993	0.991
100	0.993	0.989
200	0.993	0.991
400	0.993	0.989
800	0.993	0.990

TABLE V
COMMUNICATION DELAY UNDER DIFFERENT CHANNEL CONDITIONS

K	**PER**	**QPSK**		
		Uplink (ms)	Downlink (ms)	Round-trip (ms)
2	0.1767	34.6	34.3	68.9
3	0.0739	26.9	29.3	56.2
4	0.0143	23.3	28.2	51.5
6	0.0048	23.8	28.1	51.9
8	0	23.5	28.1	51.6
0	0.6	300	237	537

TABLE VI
COMMUNICATION DELAY UNDER DIFFERENT CHANNEL CONDITIONS

K	**PER**	**BPSK**		
		Uplink (ms)	Downlink (ms)	Round-trip (ms)
2	0.0096	30.7	55.0	85.7
3	0.0072	29.8	52.3	82.1
4	0	29.1	50.2	79.3
6	0	28.7	50.5	79.2
8	0	28.7	50.3	79.0

increases with the communication delay and that of CPPT30 remains almost unchanged. Also, according to Table IV, the change of the Jain index in both CPPT20 and CPPT30 with respect to increasing communication delay is very small. This is because all inverters cooperatively adjust surplus power of their PV systems following the coordination of the central controller and hence the fairness is insensitive to the communication delay.

In contrast to Jain index and over-voltage occurrence, four parameters for the reverse power flow given in Table III are sensitive to the variations of the round-trip communication delay. The *exceeded power* indicates the power above the reverse power threshold. The *exceeded energy* indicates the total energy corresponding to the exceeded power. The *maximum exceeded time* is the maximum time period when the reverse power exceeds the threshold. The *total exceeded time* is the total time that the reverse power exceeds the threshold. As the round-trip delay increases, all these parameters increase apparently. In CPPT20, the reverse power may exceed the threshold up to 12 KW, which severely violates the threshold and the total exceeded time is nearly doubled as the round-trip delay increases by twice. These results indicate that the reverse power flow is most significantly influenced by the round-trip delay, especially when the reverse power threshold is tighter (e.g. 20 KW in our simulation). Therefore, to control the reverse power flow properly, the round-trip delay must be reduced to a certain level.

D. Performance of the Communication Network

To determine whether the delay requirement imposed by the physical system can be achieved, several experiments are conducted to measure the round-trip delay under the network setting specified in Section VI-A. Since mesh routers and end nodes are intentionally installed in the line of sight for better link quality, Rician channel model is adopted to capture the fading effect in our simulation. To reflect different channel conditions, the K factor of Rician model varies from 2 to 8. The results for different transmission rates (corresponding to 1/2 BPSK and 1/2 QPSK) are shown in Table V and Table VI. It can be observed that the delay for 1/2 QPSK is always smaller than that of 1/2 BPSK, which means a higher transmission rate is helpful to reduce the communication delay. However, the robustness of BPSK also neutralizes the negative effect of a lower transmission rate, and hence the delay difference between two cases is small. Actually, in all cases the round-trip delays for both BPSK and QPSK are basically controlled within 100 ms. By checking the results in Section VI-C, we know that such a WMN (with either modulation) is feasible for proper operation of CPPT.

We finally consider the case when link quality is extremely poor (due to significant out-of-network interference). As shown in Table V (labeled as K = 0), the packet error rate (PER) for QPSK can reach 60%. In this case, the round-trip delay degrades to 537 ms. According to the results in Section VI-C, this delay leads to a serious reverse power flow issue.

This experiment shows the worst case scenario that definitely needs to be avoided. A possible solution to this problem is to develop a link recovery scheme based on cognitive radios. The detailed design is subject to future research. In case a link failure is permanent leading to missing messages, our CPPT scheme can still work properly as discussed in Section V-B5.

VII. Conclusion

In this paper, a framework of coordinated power point tracking (CPPT) was developed for PV systems that are connected to a distribution grid. Under this framework, power points of all PV systems in the same distribution grid are controlled via a distributed and coordinated approach. Thus, issues such as over-voltage, reverse power flow, and fairness are all resolved while output power of PV systems is maximized. Wireless networks play a critical role in CPPT, so a hierarchical WMN was designed. More importantly, two layer-2 routing protocols were developed to support proper operation of CPPT. Simulation results demonstrated the advantages of CPPT over existing schemes. The effectiveness of the hierarchical WMN and the layer-2 routing protocols was also validated. The framework of CPPT gives us insights about building other cyber-physical systems for smart grid. It also provides a systematic guideline for designing communication networks for a cyber-physical system. In the future work, the framework will be adopted to coordinate charging of electric vehicles in a distribution grid via WMNs.

Appendix A
The Proof of Lemma 1

Let P' be the sum of active power consumed by loads and power loss, so $P' = \sum_{i\in\mathcal{N}\setminus\{0\}} P_{L_i} + P_{loss}$. Based on the power balance principle, the active power generated by PV systems plus that pulled from the transformer is equal to the active power P', so $P_0+\sum_{i\in\mathcal{N}_1} P_{G_i} = \sum_{i\in\mathcal{N}\setminus\{0\}} P_{L_i}+P_{loss}$. Intuitively, to minimize P_0, we need to increase P_{G_i}, i.e., the power generated by PV systems. However, increasing P_{G_i} may lead to more power consumption, i.e., higher P'. Nonetheless, as long as the increased power of PV systems is always larger than the increment of P', then P_0 can be reduced by increasing power of PV systems until the reverse power constraint in (5) is reached or all PV systems generate the maximum output power.

To prove that the increased power of PV systems is always larger than the increment of P', we look into power generation in one PV system and its impact to P'. Considering a PV system at the connecting point i, its increased power is denoted by ΔP_{G_i}. Corresponding to this increased power, the increased power consumption is $\Delta P'$. From point i, the sub-grid can be analyzed via the Thevenin Theorem. As shown in Fig. 12, the external circuits for the PV system is replaced by a Thevenin equivalent circuit consisting of a voltage resource V_{Th} and an impedance $Z_{\text{Th}} = R_{\text{Th}}+jX_{\text{Th}}$. Let V_i and I_i be the voltage and current of the PV system. When P_{G_i} increases to $P_{G_i}+\Delta P_{G_i}$, voltage V_i and I_i become $V_i+\Delta V_i$ and $I_i+\Delta I_i$ respectively. Due to the increased current, the increased power consumption

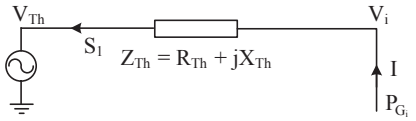

Fig. 12. Thevenin equivalent circuit for the port between i and the ground

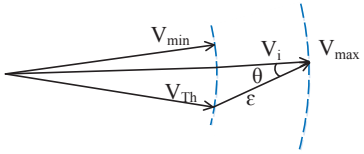

Fig. 13. Relationship among $V_i, V_{\text{Th}}, V_{\max}, V_{\min}$

$\Delta P'$ is

$$\begin{aligned}\Delta P' &= R_{\text{Th}}(|I_i+\Delta I_i|^2 - |I_i|^2),\\ &\le R_{\text{Th}}|\Delta I_i|(|I_i|+|I_i+\Delta I_i|),\\ &\le 2R_{\text{Th}}|\Delta I_i|\max(|I_i|,|I_i+\Delta I_i|).\end{aligned} \tag{8}$$

Since $\Delta I_i = \frac{\Delta V_i}{Z_{\text{Th}}}$ and $I_i = \frac{V_i - V_{\text{Th}}}{Z_{\text{Th}}}$, Eq. (8) becomes

$$\Delta P' \le 2\frac{R_{\text{Th}}}{|Z_{\text{Th}}|}\left|\frac{\Delta V_i}{Z_{\text{Th}}}\right|\max\left(|V_i+\Delta V_i - V_{\text{Th}}|, |V_i - V_{\text{Th}}|\right). \tag{9}$$

From the Thevenin equivalent circuit, we know that $V_i = V_{\text{Th}} + Z_{\text{Th}}\frac{P_{G_i}}{V_i}$ and $V_i+\Delta V_i = V_{\text{Th}} + Z_{\text{Th}}\frac{P_{G_i}+\Delta P_{G_i}}{V_i+\Delta V_i}$. Thus, we have

$$\left|\frac{\Delta V_i}{Z_{\text{Th}}}\right| = \left|\frac{\Delta P_{G_i}V_i - P_{G_i}\Delta V_i}{(V_i+\Delta V_i)V_i}\right| \le \frac{\Delta P_{G_i}|V_i| + P_{G_i}|\Delta V_i|}{|V_i+\Delta V_i||V_i|}.$$

In other words, ΔP_{G_i} satisfies

$$\Delta P_{G_i} \ge \left|\frac{\Delta V_i}{Z_{\text{Th}}}\right|\left(|V_i+\Delta V_i| - \frac{P_{G_i}|Z_{\text{Th}}|}{|V_i|}\right). \tag{10}$$

Since $P_{G_i}|Z_{\text{Th}}| = |V_i||V_i - V_{\text{Th}}|$, so Eq. (10) can be written as

$$\Delta P_{G_i} \ge \left|\frac{\Delta V_i}{Z_{\text{Th}}}\right|\left(|V_i+\Delta V_i| - |V_i - V_{\text{Th}}|\right). \tag{11}$$

Considering Eq. (9) and Eq. (11) together, we get

$$\frac{\Delta P'}{\Delta P_{G_i}} \le 2\frac{R_{\text{Th}}}{|Z_{\text{Th}}|}\frac{\max\left(|V_i+\Delta V_i - V_{\text{Th}}|, |V_i - V_{\text{Th}}|\right)}{|V_i+\Delta V_i| - |V_i - V_{\text{Th}}|}. \tag{12}$$

We know that $R_{\text{Th}} \le |Z_{\text{Th}}|$. Moreover, $|V_i+\Delta V_i| \ge V_{\min}$ and the upper bounds of $|V_i - V_{\text{Th}}|$ and $|V_i+\Delta V_i - V_{\text{Th}}|$ are the same. Define ϵ to be the upper bound of $|V_i - V_{\text{Th}}|$. Thus, Eq. (12) becomes

$$\frac{\Delta P'}{\Delta P_{G_i}} \le \frac{2\epsilon}{V_{\min}-\epsilon}. \tag{13}$$

Suppose the voltage on the impedance Z_{Th} is V_Z, so $V_i = V_{\text{Th}}+V_Z$. Thus, $|V_i - V_{\text{Th}}|$ is maximized when $V_i = V_{\max}$ and $V_{\text{Th}} = V_{\min}$, as shown in Fig. 13, where θ is the phase angle of the impedance Z_{Th}. Thus, ϵ can be calculated as follows:

$$\epsilon = V_{\max}\cos\theta - \sqrt{V_{\min}^2 - V_{\max}^2 + V_{\max}^2\cos^2\theta}. \tag{14}$$

The impedance of transmission lines is usually much smaller than that of loads, so Z_{Th} is mainly determined by the impedance of a transmission line. In Z_{Th}, X_{Th} is usually 6-8

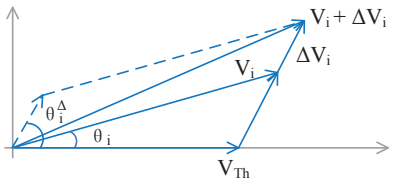

Fig. 14. Phase relationship between V_i and ΔV_i

times smaller than R_{Th} [17], so the phase angle θ is less than 10 degrees. Assuming $V_{\max}$ and $V_{\min}$ are equal to 1.1 and 0.9 of the normal voltage, respectively. Usually the voltage range is smaller [20], and then Eq. (13) is easier to satisfy. From Eq. (14), we get $\epsilon \leq 0.185V_{\max}$. Based on this result, Eq. (13) becomes

$$\frac{\Delta P'}{\Delta P_{G_i}} \leq \frac{2 \times 0.185 V_{\max}}{V_{\min} - 0.185 V_{\max}} = 0.517. \tag{15}$$

The above result indicates that, when a PV system increases output power, the increment of power consumption is always smaller than the increased power. Considering all PV systems, the same result applies. As a result, PV systems can always increase output power to reduce P_0 until the reverse power flow exceeds the threshold or all PV systems reach the maximum output power. Since the proof is independent of the power sharing among PV systems, the above result is correct under our fairness definition. This means Lemma 1 is proved.

Appendix B
The Proof of Lemma 2

This lemma implies that, whenever a PV system increases its output power, voltages in all connecting points will exceed the upper bound. Thus, proving this lemma is equivalent to proving that $\frac{\partial |V_j|}{\partial P_{G_i}} > 0$ for all $i \in \mathcal{N}_1, j \in \mathcal{N} \backslash \{0\}$.

Considering i, we first prove that $\frac{\partial |V_i|}{\partial P_{G_i}} > 0$. On the Thevenin equivalent circuit in Fig. 12, suppose $V_{\text{Th}} = |V_{\text{Th}}| \angle 0$ is the reference voltage and S_1 is the power flowing to V_{Th}. Thus, $S_1 = (P_{G_i} - R_{\text{Th}} |I|^2) - jX_{\text{Th}} |I|^2$ and $V_i = V_{\text{Th}} + \frac{S_1^*}{V_{\text{Th}}} Z_{\text{Th}}$, where S_1^* is the complex conjugate of S_1. As a result, the following equation is obtained:

$$V_i = V_{\text{Th}} + \frac{P_{G_i} R_{\text{Th}} - \left(R_{\text{Th}}^2 + X_{\text{Th}}^2\right) |I|^2}{V_{\text{Th}}} + j \frac{P_{G_i} X_{\text{Th}}}{V_{\text{Th}}}. \tag{16}$$

From this equation, we know that ΔV_i can be described as

$$\Delta V_i = \frac{R_{\text{Th}} \left(\Delta P_{G_i} - \left(1 + \frac{X_{\text{Th}}^2}{R_{\text{Th}}^2}\right) \Delta P'\right)}{V_{\text{Th}}} + j \frac{\Delta P_{G_i} X_{\text{Th}}}{V_{\text{Th}}}. \tag{17}$$

In Eq. (15), it is proved that $\Delta P' \leq 0.517 \Delta P_{G_i}$. In addition, R_{Th} is 6-8 times larger than X_{Th}. Thus, the real part of ΔV_i is positive. Thus, the phase angle of ΔV_i is within $[0, \frac{\pi}{2}]$. From Eq. (16), V_i has a positive imaginary part. Moreover, $V_{\text{Th}}^2 \gg \left(R_{\text{Th}}^2 + X_{\text{Th}}^2\right) |I|^2$, so the real part of V_i is also positive. Thus, the phase angle of V_i is also within $[0, \frac{\pi}{2}]$. As a result, both V_i and ΔV_i are within the first quadrant, which implies that $|V_i + \Delta V_i| > |V_i|$ is always satisfied. Consequently, $\frac{\partial |V_i|}{\partial P_{G_i}} > 0$.

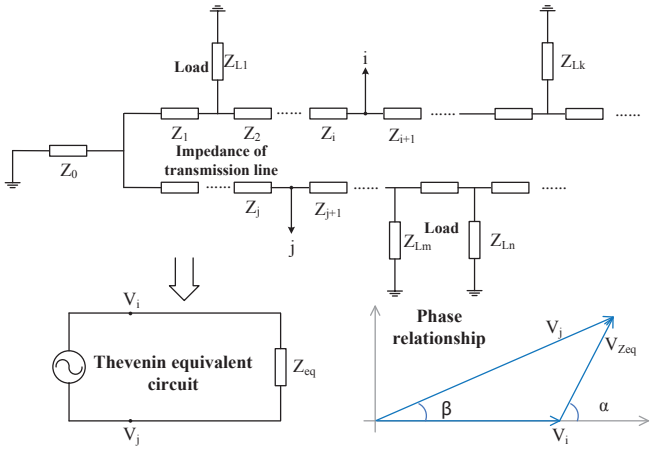

Fig. 15. Thevenin equivalent circuit for the port between i and j

Next we prove that $\frac{\partial |V_j|}{\partial P_{G_i}} > 0$ for $j \neq i$. We know that $\frac{\partial |V_j|}{\partial P_{G_i}} > 0$ is equivalent to $|V_j + \Delta V_j| > |V_j|$. Moreover, if $|\theta_j - \theta_j^{\Delta}| < \frac{\pi}{2}$, where θ_j and θ_j^{Δ} are the phase angle of $|V_j|$ and $|V_j + \Delta V_j|$, respectively, then $|V_j + \Delta V_j| > |V_j|$. Thus, $|\theta_j - \theta_j^{\Delta}| < \frac{\pi}{2}$ provides a sufficient condition to ensure $\frac{\partial |V_j|}{\partial P_{G_i}} > 0$.

Define $\Theta = |\theta_j - \theta_i| + |\theta_i - \theta_i^{\Delta}| + |\theta_i^{\Delta} - \theta_j^{\Delta}|$. Since $|\theta_j - \theta_j^{\Delta}| \leq \Theta$, so if $\Theta < \frac{\pi}{2}$, then $|\theta_j - \theta_j^{\Delta}| < \frac{\pi}{2}$, which leads to $\frac{\partial |V_j|}{\partial P_i} > 0$. We evaluate three components of Θ as follows.

Firstly, $|\theta_i - \theta_i^{\Delta}|$ is studied. As analyzed in Eqs. (16) and (17), the relationship between V_{Th}, V_i and ΔV_i is illustrated in Fig. 14, which shows that $|\theta_i - \theta_i^{\Delta}| \leq \theta_i^{\Delta}$. Moreover, the phase angle is equal to

$$\theta_i^{\Delta} = \tan^{-1} \left(\frac{X_{\text{Th}}}{R_{\text{Th}}} \frac{\Delta P_{G_i}}{\Delta P_{G_i} - \left(1 + \frac{X_{\text{Th}}^2}{R_{\text{Th}}^2}\right) \Delta P'} \right) \tag{18}$$

where $\tan^{-1}$ is the inverse tangent function. Since we know that $\frac{X_{\text{Th}}}{R_{\text{Th}}} < 1/6$ and $\Delta P' / \Delta P_{G_i} < 0.517$, so the θ_i^{Δ} is smaller than 20 degrees. Thus, $|\theta_i - \theta_i^{\Delta}|$ is also lower than 20 degrees.

Secondly, $|\theta_j - \theta_i|$ is studied. We use a Thevenin equivalent circuit to analyze the port between i and j. Since the impedance of loads is much larger than that of transmission lines, the equivalent impedance is mostly determined by the impedance of a transmission line, as shown in Fig. 15. In other words, the impedance of the Thevenin equivalent circuit in Fig. 15 has the same phase angle as a transmission line. As shown in Fig. 15, the phase difference $\beta = |\theta_j - \theta_i|$ is smaller than the phase angle α of the transmission line. Since the phase angle of a transmission line is usually smaller than 10 degrees, so $|\theta_j - \theta_i|$ is lower than 10 degrees. Similarly, $|\theta_i^{\Delta} - \theta_j^{\Delta}|$ is smaller than 10 degrees.

As a result, $\Theta = |\theta_j - \theta_i| + |\theta_i - \theta_i^{\Delta}| + |\theta_i^{\Delta} - \theta_j^{\Delta}| < 40$ degrees. In other words, $|\theta_j - \theta_j^{\Delta}| < 40$ degrees, which implies that $\frac{\partial |V_j|}{\partial P_{G_i}} > 0$ for $j \neq i$. Consequently, we have shown that $\frac{\partial |V_j|}{\partial P_{G_i}} > 0$ for all $i \in \mathcal{N}_1, j \in \mathcal{N} \backslash \{0\}$, i.e., Lemma 2 is proved.

ACKNOWLEDGMENT

The research work is supported by State Grid Corporation of China, National Natural Science Foundation of China (NSFC) No. 61172066, and Oriental Scholar Program of Shanghai Municipal Education Commission. The authors would like to thank these sponsors for their generous support.

REFERENCES

[1] T. Esram and P. L. Chapman, "Comparison of photovoltaic array maximum power point tracking techniques," *IEEE Transaction on Energy Conversion*, vol. 22, no. 2, pp. 439-449, 2007.
[2] S. Keshav, "An engineering approach to computer networking," Addison-Wesley, Reading, MA, 1997.
[3] R. Jain, D. M. Chiu, and W. R. Hawe, "A quantitative measure of fairness and discrimination for resource allocation in shared computer system," Digital Equipment Corporation Eastern Research Laboratory, 1984.
[4] E. Demirok, et al, "Clustered PV inverters in LV networks: An overview of impacts and comparison of voltage control strategies," *2009 IEEE Electrical Power and Energy Conference*, 2009.
[5] Y. Wang, et al, "Online overvoltage prevention control of photovoltaic generators in microgrids," *IEEE Transactions on Smart Grid*, vol. 3, no. 4, pp. 2071-2078, 2012.
[6] S. Anand, B. G. Fernandes, and M. Guerrero, "Distributed control to ensure proportional load sharing and improve voltage regulation in low-voltage DC microgrids," *IEEE Transactions on Power Electronics*, vol. 28, no. 4, pp. 1900-1913, 2013.
[7] J. W. Simpson-Porco, F. Dörfler, and F. Bullo, "Synchronization and power sharing for droop-controlled inverters in islanded microgrids," *Automatica*, vol. 49, no. 9, pp. 2603-2611, 2013.
[8] R. Tonkoski, L. A. C. Lopes, and T. H. M. El-Fouly, "Coordinated active power curtailment of grid connected PV inverters for overvoltage prevention," *IEEE Transactions on Sustainable Energy*, vol. 2, no. 2, pp. 139-147, 2011.
[9] E. DallAnese, H. Zhu, and G. B. Giannakis, "Distributed optimal power flow for smart microgrids," *IEEE Transactions on Smart Grid*, vol. 4, no. 3, pp. 1464-1475, Sep. 2013.
[10] A. Lam, B. Zhang, and D. N. Tse, "Distributed algorithms for optimal power flow problem," *2012 IEEE 51st Annual Conference on Decision and Control*, 2012.
[11] S. N. Liew and G. Strbac, "Maximising penetration of wind generation in exsiting distribution networks," *IEE Proceedings Generation Transmission Distribution*, vol 149, no. 3, May 2002.
[12] X. Liu, A. Aichhorn, L. Liu, and H. Li, "Coordinated control of distributed energy storage system with tap changer transformers for voltage rise mitigation under high photovoltaic penetration," *IEEE Transaction on Smart Grid*, 2012.
[13] K. Yoshida, K. Kouchi, Y. Nakanishi, H. Ota, and R. Yokoyama, "Centralized control of culstered PV generations for loss minimization and power quality," *IEEE Power and Energy Society General Meeting-Conversion and Delivery of Electrical Energy in the 21st Century*, pp. 1-6, July 2008.
[14] L. M. Cipcigan and P. C. Taylor, "Investigation of the reverse power flow requirements of high penetrations of small-scale embedded generation," *IET Renewable Power Generation*, vol. 1, no. 3, pp. 160-166, 2007.
[15] J. Lavaei and S. Low, "Convexification of optimal power flow problem," *2010 48th Annual Allerton Conference on Communication, Control, and Computing (Allerton)*, pp. 223-232, 2010.
[16] IEEE TGah Functional Requirements and Evaluation Methodology Rev.5, IEEE 802.11-11/0905r5. Available: https://mentor.ieee.org/802.11, 2012.
[17] H. Laaksonen, P. Saari, and R. Komulainen, "Voltage and frequency control of inverter based weak LV network microgrid," *2005 International Conference on Future Power Systems*, 2005.
[18] N. Femia, G. Petrone, G. Spagnuolo, and M. Vitelli, "Optimization of perturb and observe maximum power point tracking method," *IEEE Transactions on Power Electronics*, vol. 20, no. 4, pp. 963-973, July 2005.
[19] [Online]. Available: http://rredc.nrel.gov/solar/old_data/nsrdb/
[20] ANSI Std C84.1-2006, "American national standard for electric power systems and equipment - voltage ratings (60Hertz)".

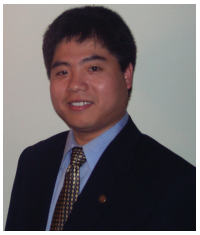

Xudong Wang is currently with the UM-SJTU Joint Institute, Shanghai Jiao Tong University. He is a distinguished professor (Shanghai Oriental Scholar) and is the director of the Wireless and NetworkinG (WANG) Lab. He is also an affiliate faculty member with the Electrical Engineering Department at the University of Washington. Since he received the Ph.D. degree in Electrical and Computer Engineering from Georgia Institute of Technology in August 2003, he has been working as a senior research engineer, senior network architect, and R&D manager in several companies. He has been actively involved in R&D, technology transfer, and commercialization of various wireless networking technologies. His research interests include wireless communication networks, smart grid, and cyber physical systems. He holds a number of patents on wireless networking technologies and most of his inventions have been successfully transferred to products. Dr. Wang is an editor for *IEEE Transactions on Vehicular Technology*, Elsevier *Ad Hoc Networks*, and ACM/Kluwer *Wireless Networks*. He was also a guest editor for several journals. He was the demo co-chair of the ACM International Symposium on Mobile Ad Hoc Networking and Computing (ACM MOBIHOC 2006), a technical program co-chair of Wireless Internet Conference (WICON) 2007, and a general co-chair of WICON 2008. Dr. Wang is a senior member of IEEE and was a voting member of IEEE 802.11 and 802.15 Standard Committees.

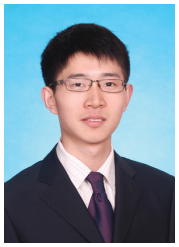

Yibo Pi received the B.S. degree in Electrical and Computer Engineering from Shanghai Jiao Tong University (SJTU), Shanghai, China, in 2012. He is currently a M.S. student with the University of Michgan-Shanghai Jiao Tong University Joint Institute, SJTU. His current research interests include smart grid communications and wireless networks.

Wenguang Mao received the B.S. degree in Electrical and Computer Engineering from Shanghai Jiao Tong University (SJTU), Shanghai, China, in 2011 and the M.S. degree in Information and Communication Engineering from SJTU in 2014. His current research interests include physical-layer cooperative coding and mobile computing.

Hua Huang received the Master degree in Electrical Engineering from Shanghai Jiao Tong University, Shanghai, China, in 1995. Since then he has been a senior engineer and a manager in the State Grid Company of China. Since June 2012 he has been elected as a leading expert of China State Grid, specializing in the power equipment maintenance. His research interests include condition monitoring and fault diagnosis of power equipment.